Journal of Sound and Vibration (2001) **245**(3), 527–544
doi:10.1006/jsvi.2001.3569, available online at http://www.idealibrary.com on IDEAL®

FREE VIBRATION OF LAYERED PIEZOELECTRIC SPHERICAL CAPS

Y.-C. Wu and P. Heyliger

Department of Civil Engineering, Colorado State University, Fort Collins, CO 80523-1372, *U.S.A.*

(*Received* 25 *February* 2000, *and in final form* 22 *January* 2001)

The free asymmetric and axisymmetric vibration of layered piezoelectric spherical shells are analyzed using a two-dimensional first order shear deformable shell theory. Piecewise Hermite interpolation polynomials are used to approximate the unknowns in the azimuthal direction, to Fourier approximations in the circumferential direction. Natural frequencies for layered elastic caps were computed and found to be in close agreement with other studies and results from a discrete-layer model of the equations of linear elasticity. Several new results are calculated for layered piezoelectric spherical caps with clamped and hinged boundary conditions.

1. INTRODUCTION

Spherical shells and spherical caps have been studied intensively for purely elastic media. Naghdi [1, 2] has investigated the small axisymmetric deformation of elastic shells of revolution and the formulation of suitable stress–strain relations and the appropriate boundary conditions. Johnson and Reissner [3] examined transverse vibrations of shallow spherical shells. Hoppmann [4] provided direct solutions of the determinantal frequency equation for clamped and simply boundary conditions. Kalnins and Naghdi [5] discovered the axisymmetric and asymmetric vibrations of thin elastic spherical shells. Mukherjee [6] computed the stresses due to vibration of spherical shells. By the use of suitable auxiliary variables, the equations of motion of non-shallow spherical shells were reduced by Prasad [7] to a system of two uncoupled and one partly coupled equations. Frequency equations were also derived by Kalnins [8] in terms of Legendre functions with complex indices. The Holzer method has been generalized by Zarghamee and Robinson [9] to the analysis of free vibration of spherical shells. Rath and Das [10, 11] derived the general equations of motion including the effect of shear deformations and obtained the natural frequencies for the axisymmetric motion of closed symmetrically layered orthotropic spherical shells. A finite ring shell element was developed by Venkataramana and Venkateswara [12]. The free vibrations of isotropic spherical shells were investigated by De Souza and Croll [13] using a variational development of the equations of motion based upon classical shell theory. Kunieda [14] studied flexural axisymmetric free vibrations of a spherical dome. Free asymmetric vibration of spherical shells with clamped and hinged boundary conditions were analyzed using the finite element method by Mirza and Singh [15]. Tessler and Spiridigliozzi [16] studied resolving membrane and shear locking phenomena in curved shear-deformable axisymmetric shell elements. Axisymmetric free vibration of moderately thick polar orthotropic hemispherical shells were studied by Chao *et al.* [17] under various boundary conditions with sliding, guided pin, clamped and hinged edges. Gautham and

0022-460X/01/330527 + 18 $35.00/0

Ganesan [18] studied free vibration characteristics of isotropic and laminated orthotropic spherical caps.

To the authors' knowledge, no studies exist for the analysis of piezoelectric spherical caps. This configuration can be used in a wide variety of applications including adaptive smart membranes and active shells, frequency analysis of laminated transducers and sensors, and the design of artificial heart pumps and robotic surgery instruments. In the present study, the equations of motion and the charge equation of electrostatics are considered in variational form using the piezoelectric constitutive equations and stress–strain relations in spherical co-ordinates. Substituting these equations into Hamilton's principle yields a weak form which forms the fundamental basis for our numerical analyses. A two-dimensional first order shear deformation model for piezoelectric shells is generated. Displacements and potential are expressed in terms of the mid-surface displacements and independent rotations. Piecewise Hermite interpolation polynomials are used in the azimuthal direction with Fourier approximations in the circumferential direction. The results are compared with those from a three-dimensional Ritz approximation [19], in which piecewise quadratic Lagrange interpolation polynomials are used in the radial direction with Fourier approximations in the circumferential and azimuthal directions.

Using the present model, the natural frequencies for purely elastic shells with a wide geometric range have been computed and found to be in close agreement with results from literature. Several new results for layered piezoelectric caps with clamped and hinged boundary conditions have been calculated using the first order deformation method, and we discuss the general implications of these results. Further, we demonstrate that the first order shear deformation theory is less computationally intensive than continuum theories, and also gives good solutions for thin shells.

2. THEORY

In this section, the governing equations for linear piezoelectricity are presented, and the two-dimensional first order shear deformation approximations to these equations are derived for piezoelectric caps in spherical co-ordinates.

2.1. GOVERNING EQUATIONS OF LINEAR PIEZOELECTRICITY

In spherical co-ordinates, the displacement components are defined in the radial ($x_1 = r$), azimuthal ($x_2 = \zeta$), and circumferential ($x_3 = \theta$) directions as shown in Figure 1. These displacement components are denoted by $U = U_r = u(r, \zeta, \theta)$, $V = U_\zeta = v(r, \zeta, \theta)$ and $W = U_\theta = w(r, \zeta, \theta)$, with the electrostatic potential given as $\phi = \phi(r, \zeta, \theta)$.

The piezoelectric constitutive equations for any layer in the spherical caps are given by Tiersten [20] as

$$\sigma_i = C_{ij} S_j - e_{ki} E_k, \qquad D_k = e_{kj} S_j + \varepsilon_{kl} E_l. \tag{1, 2}$$

Here $i, j = 1, \ldots, 6$ and $l, k = 1, 2, 3$, σ_i are the components of the stress tensor, C_{ij} are the components of the elastic tensor, S_j are the components of the strain tensor, e_{ki} are the piezoelectric coefficients, E_k are the components of the electric field, D_k are the components of the electric displacement, and ε_{kl} are the dielectric constants, and the single subscript for the stress components represents the contracted double subscript notation in a standard form, such as $11 = 1$, $22 = 2$, $33 = 3$, $23 = 4$, $13 = 5$, and $12 = 6$. The rotated elastic stiffnesses are given by $C_{11}, C_{22}, C_{33}, C_{44}, C_{55}, C_{66}, C_{12}, C_{13}$, and C_{23}. The non-zero

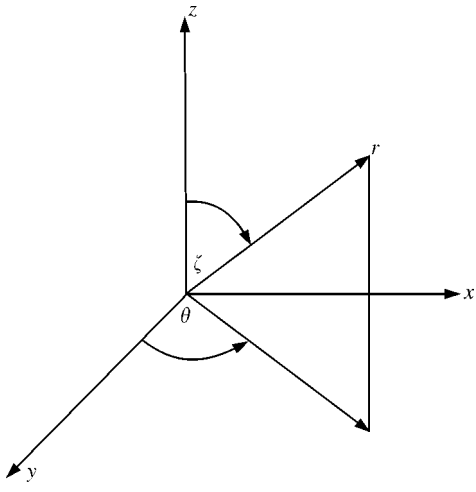

Figure 1. Notation of spherical co-ordinates.

elastic coefficients are given as $e_{11}, e_{12}, e_{13}, e_{26}$, and e_{35}. The non-zero dielectric constants are $\varepsilon_{11}, \varepsilon_{22}$, and ε_{33}. The constitutive relations of an orthotropic material are assumed in this study, and the piezoelectric layers are poled in the radial direction.

The weak form of the equations of motion for the shell can be written using Hamilton's principle for a linear piezoelectric medium in spherical co-ordinates. This forms the basis of the approximate model presented in the sequel. Hamilton's principle is given by Tiersten [20] as

$$\delta \int_{t0}^{t1} \mathrm{d}t \int_{v} [\tfrac{1}{2}\rho \dot{u}_i \dot{u}_i - H(S_{kl}, E_k)]\,\mathrm{d}V + \int_{t0}^{t1} \mathrm{d}t \int_{s} (\bar{T}_i \delta u_i - \bar{Q}\delta\phi)\,\mathrm{d}s = 0. \tag{3}$$

Here t_0 and t_1 are two arbitrary times, δ is the variational operator, V and S are the volume and surface of the solid, $\bar{T}_i$ and $\bar{Q}$ represent specified traction and surface charges, and H is the electric enthalpy per unit volume, given in terms of the strain and electric-field components as

$$H(S_i, E_k) = \tfrac{1}{2}C_{ij}S_iS_j - e_{ki}E_kS_i - \tfrac{1}{2}\varepsilon_{kl}E_kE_l. \tag{4}$$

The strain–displacement relations can be written [21] in spherical co-ordinates as

$$S_{rr} = \frac{\partial u}{\partial r}, \qquad S_{\zeta\zeta} = \frac{1}{r}\frac{\partial v}{\partial \zeta} + \frac{u}{r}, \tag{5, 6}$$

$$S_{\theta\theta} = \frac{1}{r\sin\zeta}\frac{\partial w}{\partial \theta} + \frac{\cot\zeta}{r}v + \frac{u}{r}, \qquad S_{\zeta\theta} = \frac{1}{r\sin\zeta}\frac{\partial v}{\partial \theta} + \frac{1}{r}\frac{\partial w}{\partial \zeta} - \frac{\cot\zeta}{r}w, \tag{7, 8}$$

$$S_{r\theta} = \frac{1}{r\sin\zeta}\frac{\partial u}{\partial \theta} + \frac{\partial w}{\partial r} - \frac{w}{r}, \qquad S_{r\zeta} = \frac{1}{r}\frac{\partial u}{\partial \zeta} + \frac{\partial v}{\partial r} - \frac{v}{r}. \tag{9, 10}$$

Here S_{rr}, $S_{\theta\theta}$, $S_{\zeta\zeta}$ are the components of the linear strain tensor, and $S_{r\zeta}$, $S_{\zeta\theta}$, $S_{r\theta}$ are the components of engineering shear strain. The electric field components E_i are related to the

electrostatic potential $\phi(r, \zeta, \theta)$ using the relations

$$E_{rr} = -\frac{\partial \phi}{\partial r}, \qquad E_{\zeta\zeta} = -\frac{1}{r}\frac{\partial \phi}{\partial \zeta}, \qquad E_{\theta\theta} = -\frac{1}{r \sin \zeta}\frac{\partial \phi}{\partial \theta}. \tag{11–13}$$

2.2. FIRST ORDER SHEAR DEFORMATION THEORY APPROXIMATIONS

The hypothesis of classical shell theory is that straight lines normal to the mid-surface remain straight, normal and unchanged in length after deformation. The requirement of normality is usually deleted in first order shear deformation theory (FSDT). The geometry of the shell considered in this study is a surface of revolution with an arbitrarily curved meridian. The notation for the co-ordinates is shown in Figure 2. The displacement components at a distance z away from the shell mid-surface are expressed in terms of mid-surface displacements and independent rotations of the normal as

$$U(r, \zeta, \theta) = \hat{u}(\zeta, \theta), \qquad V(r, \zeta, \theta) = \hat{v}(\zeta, \theta) + z\hat{\alpha}(\zeta, \theta), \tag{14, 15}$$

$$W(r, \zeta, \theta) = \hat{w}(\zeta, \theta) + z\hat{\beta}(\zeta, \theta), \qquad \phi(r, \zeta, \theta) = \hat{\phi}(\zeta, \theta). \tag{16, 17}$$

We base our assumption of constant potential through the thickness on the small differences between open and closed circuit boundary conditions for the top and bottom faces for typical laminates [22]. This implies that the radial component of the electric field is 0. This significantly reduces the number of unknowns, while the influence of the surface boundary condition has been shown to be small as long as the shell is relatively thin. We denote U, V, W as the displacements of any point in the r, ζ and θ directions, respectively, and $\hat{u}$, $\hat{v}$, $\hat{w}$ as the corresponding mid-surface displacements. We use $\hat{\phi}$ to denote the corresponding mid-surface electrostatic potential, with $\hat{\alpha}$ and $\hat{\beta}$ the rotations of the normal in azimuthal and circumferential directions.

The displacements $\hat{u}$, $\hat{v}$, $\hat{w}$, $\hat{\alpha}$, $\hat{\beta}$ and the electrostatic potential $\hat{\phi}$ can be described by Fourier series expansions in the circumferential direction [15] as

$$\hat{u}(\zeta, \theta) = \sum_{N=0}^{\infty} f_{\hat{u}}(\zeta)\cos(N\theta), \qquad \hat{v}(\zeta, \theta) = \sum_{N=0}^{\infty} f_{\hat{v}}(\zeta)\cos(N\theta), \tag{18, 19}$$

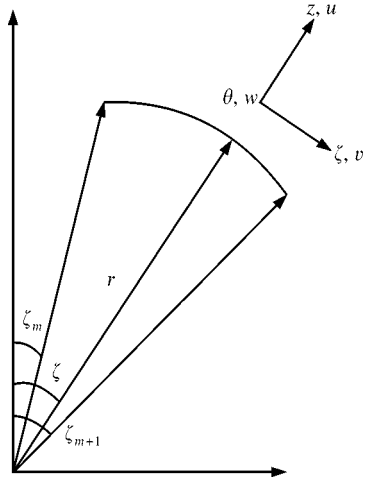

Figure 2. Notation of co-ordinates and displacements for FSDT.

$$\hat{w}(\zeta, \theta) = \sum_{N=1}^{\infty} f_{\hat{w}}(\zeta) \sin(N\theta), \qquad \hat{\alpha}(\zeta, \theta) = \sum_{N=0}^{\infty} f_{\hat{\alpha}}(\zeta) \cos(N\theta), \tag{20, 21}$$

$$\hat{\beta}(\zeta, \theta) = \sum_{N=1}^{\infty} f_{\hat{\beta}}(\zeta) \sin(N\theta), \qquad \hat{\phi}(\zeta, \theta) = \sum_{N=1}^{\infty} f_{\hat{\phi}}(\zeta) \cos(N\theta). \tag{22, 23}$$

Here the functions $f_{\hat{u}}, f_{\hat{v}}, f_{\hat{w}}, f_{\hat{\alpha}}, f_{\hat{\beta}}, f_{\hat{\phi}}$ that represent the variation in the azimuthal direction at any point between the nodes of the element are represented as in reference [15] in Hermite polynomial form as

$$f_u(\zeta) = [f_1(X)\hat{u}^{(m)} + f_2(X)\hat{u}_{,\zeta}^{(m)} + f_3(X)\hat{u}^{(m+1)} + f_4(X)\hat{u}_{,\zeta}^{(m+1)}], \tag{24}$$

where m is the element number. Similarly, $f_{\hat{v}}, f_{\hat{w}}, f_{\hat{\alpha}}, f_{\hat{\beta}}, f_{\hat{\phi}}$ can be expressed in terms of the functions $f_1(\zeta)$ through $f_4(\zeta)$ by inserting the appropriate parameters $\hat{v}$, $\hat{w}$, $\hat{\alpha}$, $\hat{\beta}$, $\hat{\phi}$ in place of $\hat{u}$. The functions $f_i(X)$, $i = 1 \ldots 4$ are given by Singh and Mirza [15] as

$$f_1(X) = (1 - X)^2(1 + 2X), \qquad f_2(X) = \zeta_e X(1 - X)^2, \tag{25, 26}$$

$$f_3(X) = 1 - (1 - X)^2(1 + 2X), \qquad f_4(X) = -\zeta_e X^2(1 - X). \tag{27, 28}$$

Here $X = (\zeta - \zeta_m)/(\zeta_{m+1} - \zeta_m)$, $\zeta_e = \zeta_{m+1} - \zeta_m$, and ζ_m is the azimuthal element.

Substituting these displacement components into the strain–displacement and field-potential relations of equations (5)–(13) yields these relations in terms of mid-surface displacements and rotations. Substituting these relations into Hamilton's principle yields the corresponding weak form. These resulting terms have been integrated through the thickness to eliminate the dependence on r using a shear correction factor of 5/6 [18]. Substituting the approximate displacements and their variations into the weak forms and collecting terms allows for writing the final equation for periodic harmonic motions in terms of the periodic frequency ω in matrix form as

$$\omega^2 \begin{bmatrix} [M^{11}] & [0] & [0] & [0] & [0] & [0] \\ [0] & [M^{22}] & [0] & [M^{24}] & [0] & [0] \\ [0] & [0] & [M^{33}] & [0] & [M^{35}] & [0] \\ [0] & [M^{42}] & [0] & [M^{44}] & [0] & [0] \\ [0] & [0] & [M^{53}] & [0] & [M^{55}] & [0] \\ [0] & [0] & [0] & [0] & [0] & [0] \end{bmatrix} \begin{Bmatrix} \{\hat{u}\} \\ \{\hat{v}\} \\ \{\hat{w}\} \\ \{\hat{\alpha}\} \\ \{\hat{\beta}\} \\ \{\hat{\phi}\} \end{Bmatrix}$$

$$+ \begin{bmatrix} [K^{11}] & [K^{12}] & [K^{13}] & [K^{14}] & [K^{15}] & [K^{16}] \\ [K^{21}] & [K^{22}] & [K^{23}] & [K^{24}] & [K^{25}] & [K^{26}] \\ [K^{31}] & [K^{32}] & [K^{33}] & [K^{34}] & [K^{35}] & [K^{36}] \\ [K^{41}] & [K^{42}] & [K^{43}] & [K^{44}] & [K^{45}] & [K^{46}] \\ [K^{51}] & [K^{52}] & [K^{53}] & [K^{54}] & [K^{55}] & [K^{56}] \\ [K^{61}] & [K^{62}] & [K^{63}] & [K^{64}] & [K^{65}] & [K^{66}] \end{bmatrix} \begin{Bmatrix} \{\hat{u}\} \\ \{\hat{v}\} \\ \{\hat{w}\} \\ \{\hat{\alpha}\} \\ \{\hat{\beta}\} \\ \{\hat{\phi}\} \end{Bmatrix} = \begin{Bmatrix} \{0\} \\ \{0\} \\ \{0\} \\ \{0\} \\ \{0\} \\ \{0\} \end{Bmatrix}. \tag{29}$$

Matrix condensation is employed to transform the matrix to the general eigenvalue problem which we solve using the QR algorithm. The explicit forms of the coefficient matrices are given in Appendix A.

2.3. DISCRETE-LAYER MODEL

A three-dimensional Ritz discrete-layer approximation method is used in this study for purposes of comparison for the case of purely elastic shells. Piecewise quadratic Lagrange interpolation polynomials are used in the radial direction with Fourier approximations in the circumferential and azimuthal directions. The governing equations and computational procedures are derived in reference [19], but are not included here.

2.4. BOUNDARY CONDITIONS

2.4.1. *FSDT*

Using the first order shear deformation theory (FSDT), it is a simple method to set boundary conditions corresponding to a clamped edge and a hinged edge. These are given as (1) $\hat{u} = \hat{v} = \hat{w} = \hat{u}_{,\zeta} = \hat{\alpha} = \hat{\beta} = \hat{\phi} = 0$ for the clamped edge, and (2) $\hat{u} = \hat{v} = \hat{w} = \hat{\phi} = 0$ for the hinged edge.

In this study, only axisymmetric and asymmetric frequencies are considered. Axisymmetric response implies symmetry about $\zeta = 0$ with $V = 0$ everywhere in the shell. Asymmetric response implies antisymmetry about $\zeta = 0$.

2.4.2. *Discrete-layer model*

The boundary conditions for clamped shells in our analytic model using the Ritz method [19] are $U = V = W = \phi = 0$. The harmonic solutions of the axisymmetric case for a clamped shell of opening angle β deg defined in Figure 3 can be expressed in terms of the displacements and potential as

$$U = u(r, \zeta, \theta) = \sum_{M=1}^{\infty} f_r(r) \sin M(\zeta - \beta), \tag{30}$$

$$V = v(r, \zeta, \theta) = \sum_{M=1}^{\infty} f_\zeta(r) \sin M(\zeta - \beta), \tag{31}$$

$$W = w(r, \zeta, \theta) = 0{\cdot}0, \tag{32}$$

$$\phi = \phi(r, \zeta, \theta) = \sum_{M=1}^{\infty} f_\phi(r) \sin M(\zeta - \beta). \tag{33}$$

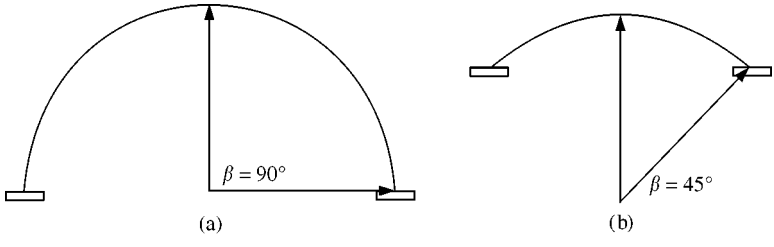

Figure 3. Configuration of (a) a deep shell ($\beta = 90°$) and (b) a shallow shell ($\beta = 45°$).

The harmonic solutions of the asymmetric case for a clamped shell of opening angle β can be expressed as

$$U = u(r, \zeta, \theta) = \sum_{N=0}^{\infty} \sum_{M=1}^{\infty} f_r(r) \sin M(\zeta - \beta) \cos N\theta, \tag{34}$$

$$V = v(r, \zeta, \theta) = \sum_{N=0}^{\infty} \sum_{M=1}^{\infty} f_\zeta(r) \sin M(\zeta - \beta) \cos N\theta, \tag{35}$$

$$W = w(r, \zeta, \theta) = \sum_{N=1}^{\infty} \sum_{M=1}^{\infty} f_\theta(r) \sin M(\zeta - \beta) \sin N\theta, \tag{36}$$

$$\phi = \phi(r, \zeta, \theta) = \sum_{N=0}^{\infty} \sum_{M=1}^{\infty} f_\phi(r) \sin M(\zeta - \beta) \cos N\theta. \tag{37}$$

We substitute these displacements into Hamilton's principle and proceed as in reference [19]. We omit these details, as the resulting equations and solutions closely follow this previous work.

3. RESULTS AND DISCUSSION

In this section, we study the free vibration response of layered elastic caps using the first order shear deformation theory and compare these results with those of a Ritz discrete layer method [19] and those reported by others [16, 18]. Axisymmetric and asymmetric frequencies for an isotropic shell are computed first and are compared with results from other studies to check the accuracy of these two methods. We then use the first order shear deformation theory to analyze natural frequencies of layered piezoelectric shells with clamped and hinged boundary conditions.

3.1. VALIDATION OF RESULTS: ISOTROPIC SHELLS

The axisymmetric frequencies of a clamped isotropic hemispherical shell with $h/a = 0{\cdot}1$ are calculated using first order shear deformation theory and the Ritz discrete layer method [19], and compared with the results of references [16, 18]. Mild steel is considered for the example of an isotropic shell. Its properties are given by $E = 2{\cdot}1 \times 10^{11}$ N/m^2, $\nu = 0{\cdot}3$. The first issue is that the accuracy of natural frequencies computed using the FSDT depends on the number of azimuthal elements used to represent the shell. In other words, convergence of the solutions is a function of the element number. Figure 4 shows that natural frequencies are highly precise when the number of azimuthal elements is 10, so the number of elements used in azimuthal direction for the following cases is 10. That means the degrees of freedom in the whole system are 110. Then, the non-dimensional frequency parameter Ω is given by $\omega R\sqrt{\rho(1 - \nu^2)/E}$. Here ω is the frequency, R is the radius of the cap, and ρ is the density. These values are given in Table 1. We also show the asymmetric frequencies of a clamped 60° mild steel shell and compare them with the results of references [15, 18]. These values are shown in Table 2, and are in good agreement (within 3%) with these earlier studies.

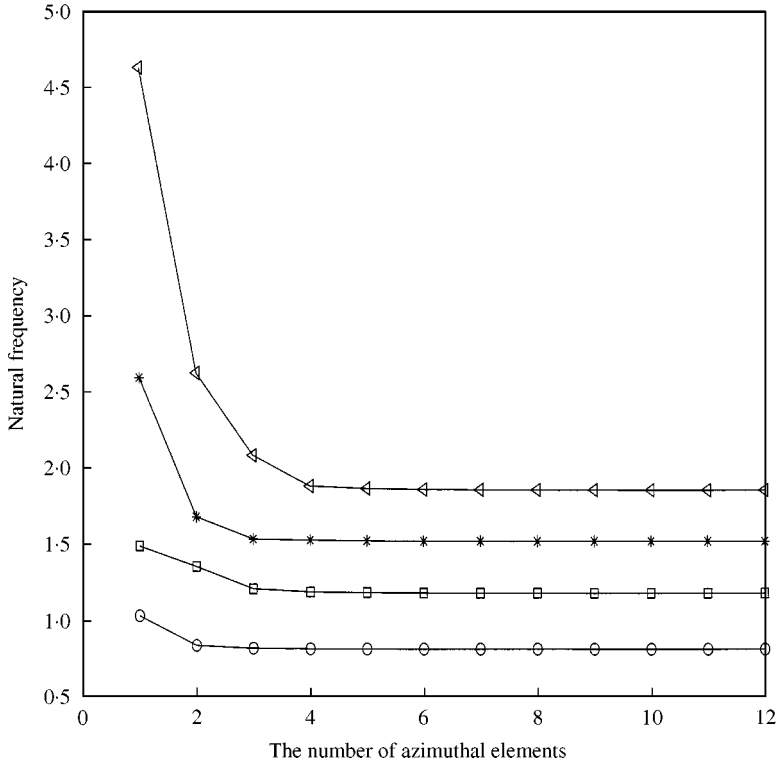

Figure 4. Convergence of the solutions: ○, mode 1; □, mode 2; ∗, mode 3; ◁, mode 4.

TABLE 1

Comparison of non-dimensional axisymmetric frequencies of an isotropic clamped hemispherical cap

Mode	1	2	3	4
FSDT	0·809	1·177	1·518	1·855
Ritz	0·814	1·185	1·527	1·884
Reference [16]	0·809	1·176	1·517	1·854
Reference [18]	0·805	1·175	1·508	1·838

3.2. ELASTIC LAYERED SHELLS

Natural frequencies for two-layer clamped elastic caps are calculated using the first order shear deformation theory and the Ritz discrete layer method. In the present study, an aluminum alloy and steel are used. The properties of the aluminum alloy are given by $E = 7{\cdot}0 \times 10^{10}\,\mathrm{N/m^2}$, $\nu = 0{\cdot}33$, $\rho = 2{\cdot}71 \times 10^3\,\mathrm{kg/m^3}$. The properties of steel are given by $E = 2{\cdot}0 \times 10^{11}\,\mathrm{N/m^2}$, $\nu = 0{\cdot}29$, $\rho = 7{\cdot}85 \times 10^3\,\mathrm{kg/m^3}$. The non-dimensional frequency Ω is given by $\omega R\sqrt{\rho/\bar{A}_{22}}$, where $\bar{A}_{22} = (\sum_{k=1}^{2} \int_{h_k}^{h_{k+1}} Q_{22}^k r^2\,\mathrm{d}r)/(\sum_{k=1}^{2} \int_{h_k}^{h_{k+1}} r^2\,\mathrm{d}r)$. Non-dimensional frequencies are computed for the opening angles 45, 60 and 90°. The thickness-to-radius ratio (h/a) considered in this example is 0·05. The thicknesses of the two layers are identical. The results are given in Table 3. The horizontal mode number indicates the N value of

TABLE 2

Comparison of non-dimensional asymmetric frequencies of an isotropic clamped 60° cap

Mode	1,1	1,2	2,1	2,2	4,1	4,2
FSDT	0·857	1·153	1·029	1·407	1·328	2·004
Ritz	0·860	1·164	1·032	1·425	1·341	2·044
Reference [15]	0·858	1·154	1·025	1·397	1·329	2·006
Reference [18]	0·853	1·145	1·029	1·408	1·325	1·994

TABLE 3

Comparison of solutions of FSDT and Ritz method for two-layer clamped mild steel spherical shells ($h/a = 0{\cdot}05$, $\nu = 0{\cdot}3$)

Mode P	N	1	2	3	4	5	6
				(a) 45°			
1	Ritz	1·0267	1·2156	1·4588	1·7773	2·2354	2·6085
	FSDT	1·0104	1·2075	1·4476	1·7626	2·1462	2·5892
2	Ritz	1·5878	1·9875	2·4725	3·0049	3·8844	4·1913
	FSDT	1·5298	1·9600	2·4349	2·9630	3·5380	4·1542
3	Ritz	2·5294	3·1568	3·8160	4·5015	5·2543	5·9416
	FSDT	2·4353	3·1378	3·7891	4·4701	5·1814	5·9212
4	Ritz	2·8905	4·0317	5·1831	6·1835	7·2115	7·8419
	FSDT	2·7777	4·0108	5·1533	6·1431	6·9977	7·8389
5	Ritz	4·0025	4·6885	5·4586	6·3088	7·3954	8·2526
	FSDT	3·9197	4·6675	5·4458	6·3012	7·2586	8·2213
				(b) 60°			
1	Ritz	0·8650	1·0285	1·1430	1·3012	1·5075	1·7642
	FSDT	0·8549	1·0210	1·1386	1·2934	1·4962	1·7466
2	Ritz	1·1505	1·4167	1·6534	1·9591	2·3012	2·6870
	FSDT	1·1305	1·3641	1·6179	1·9145	2·2532	2·6303
3	Ritz	1·6773	2·1051	2·4147	2·8400	3·2857	3·7734
	FSDT	1·6155	1·9867	2·3683	2·7810	3·2248	3·6977
4	Ritz	2·1306	3·0436	3·4005	3·9182	4·4396	5·0142
	FSDT	2·1129	2·8223	3·3268	3·8335	4·3607	4·9099
5	Ritz	2·6646	3·3099	3·9716	4·7796	5·5535	6·3143
	FSDT	2·4782	3·1265	3·9616	4·7631	5·5283	6·2217
				(c) 90°			
1	Ritz	0·5732	0·8784	0·9531	1·0189	1·1021	1·2138
	FSDT	0·5619	0·8773	0·9555	1·0226	1·1065	1·2172
2	Ritz	0·9054	1·0290	1·1307	1·2517	1·3969	1·5786
	FSDT	0·8993	1·0140	1·1174	1·2343	1·3792	1·5553
3	Ritz	1·0874	1·2511	1·3988	1·5896	1·7973	2·0477
	FSDT	1·0776	1·2235	1·3843	1·5664	1·7756	2·0125
4	Ritz	1·3684	1·6233	1·8019	2·0526	2·3076	2·6186
	FSDT	1·3436	1·5554	1·7788	2·0211	2·2866	2·5756
5	Ritz	1·6374	2·0892	2·3125	2·6188	2·9084	3·2775
	FSDT	1·6285	1·9928	2·2869	2·5827	2·8963	3·2295

Fourier approximations in the circumferential direction, with the vertical mode number corresponding to azimuthal modes P. In general, the frequencies predicted from the Ritz method are approximately 8–9% larger than the results of first order shear deformation

theory (FSDT), which can be attributed in part to the assumed shear correction factors in the FSDT model. As the angle ϕ increases, the results are in better agreement, possibly indicating that the shear terms tend to dominate the deformation as the opening angle increases.

3.3. PIEZOELECTRIC SHELLS

The first order shear deformation theory is used to calculate natural frequencies of single-layer orthotropic and piezoelectric pinned caps with an opening angle of 45°. The non-dimensional frequency Ω is given by $\omega R\sqrt{\rho/Q_{22}}$, where Q_{22} is the standard plane stress reduced stiffness. The thickness-to-radius ratio (h/a) considered in this example is 0·05. The material PZT-5 is used for the piezoelectric cap with the properties given in Table 4.

TABLE 4

Material properties for piezoelectric materials

Property	PZT-5	(Pb) (CoW)TiO_3
ρ(kg/m^3)	7570	5900
C_{11}(GPa)	111·0	128·0
C_{22}	120·0	150·0
C_{44}	22·6	56·5
C_{55}	21·1	55·2
C_{12}	75·1	32·3
C_{23}	75·2	32·3
Q_{22}	69·2	141·8
Q_{23}	24·4	288·9
Q_{44}	22·6	56·5
Q_{55}	17·6	46·0
e_{11}(C/m^2)	15·78	8·5
e_{12}	− 5·35	1·61
e_{26}	12·29	3·89
ε_{11}(C^2/N m^2)	1·53e-8	2·11e-9

TABLE 5

Natural frequencies for single-layer pinned 45° *orthotropic and piezoelectric shells* ($h/a = 0{\cdot}05$)

Mode	N	1	2	3	4	5	6
P	Caps						
1	Elastic	0·954	1·133	1·343	1·635	2·005	2·441
	Piezoelectric	1·761	3·549	4·941	6·020	6·999	7·941
2	Elastic	1·386	1·796	2·265	2·793	3·371	3·990
	Piezoelectric	2·732	4·367	6·077	7·554	8·854	10·041
3	Elastic	2·322	2·962	3·613	4·298	5·012	5·752
	Piezoelectric	2·983	5·089	6·741	8·793	10·392	11·583
4	Elastic	2·738	3·960	5·037	5·974	6·817	7·650
	Piezoelectric	3·816	5·488	7·947	9·367	11·104	13·213
5	Elastic	3·741	4·489	5·273	6·127	7·047	7·969
	Piezoelectric	3·984	6·629	8·316	10·508	12·422	14·948

To compute the influence of the piezoelectric coefficients, we first set the piezoelectric coefficients of PZT-5 zero to mimic a purely orthotropic elastic shell. We then include them in the analysis. The results are shown in Table 5. Generally, the frequencies of the piezoelectric cap are roughly 6–50% larger than the results of the orthotropic shell with the larger differences occurring for the layer circumferential and azimuthal modes. As the mode numbers increase, the influence of the piezoelectric effect is significantly reduced. Therefore, piezoelectricity has a significant effect of the free vibration of spherical shells for the material used in this study.

Natural frequencies of single-layer clamped PZT-5 caps are computed for opening angles 45, 60 and 90° to cover a wide geometric range from shallow to deep spherical shells. The thickness-to-radius ratio (h/a) considered in these examples is 0·005. The solutions are shown in Table 6. The frequencies of the 90° shells are approximately as much as 75% of

TABLE 6

Natural frequencies for single-layer, clamped piezoelectric shells ($h/a = 0{\cdot}005$)

Mode N	1	2	3	4	5	6
P						
			(a) 45°			
1	1·2635	2·2513	3·5196	4·7644	5·8181	6·9429
2	1·4137	2·5262	4·1501	5·8407	6·9976	7·9435
3	1·6048	2·9709	4·7662	6·0548	7·4097	8·8681
4	1·8446	3·4749	4·8962	6·3549	8·5967	10·0456
5	2·0546	3·8475	5·1939	7·0368	8·8376	10·8363
6	2·3605	4·0954	5·8851	7·6450	9·1224	11·3901
7	2·5752	4·3917	6·3523	8·3277	10·3863	11·6483
8	2·9189	4·9985	6·9575	9·1566	10·6667	12·8282
9	3·2551	5·2642	7·1606	9·3077	11·8585	13·5458
10	3·5526	5·5535	7·9884	9·7197	12·2013	14·5549
			(b) 60°			
1	1·0429	1·6918	2·5887	3·4363	4·1956	5·0417
2	1·1635	1·8766	3·0982	4·2967	5·3404	6·0988
3	1·2354	2·2045	3·3847	4·5723	5·4089	6·4729
4	1·3869	2·5907	3·6561	4·7236	6·4724	7·7134
5	1·4874	2·7879	3·9049	5·1965	6·6000	7·9722
6	1·6606	2·9498	4·3399	5·8122	6·9094	8·6283
7	1·8912	3·3107	4·7779	6·2261	7·7730	8·9104
8	2·0960	3·6433	5·1312	6·7056	8·0335	9·5109
9	2·3645	3·8074	5·2156	6·9862	8·8539	10·2370
10	2·5399	4·1077	5·8749	7·2525	9·0194	10·8141
			(c) 90°			
1	0·6952	1·2751	1·8302	2·3153	2·8083	3·3785
2	0·9995	1·3985	2·1641	2·9058	3·5881	4·2992
3	1·0187	1·5883	2·3176	3·1858	3·8022	4·3844
4	1·0759	1·8071	2·5055	3·3240	4·4092	5·2794
5	1·1128	1·8569	2·6881	3·5190	4·5849	5·5003
6	1·2057	2·0286	2·9433	4·0137	4·8942	6·0745
7	1·2737	2·2512	3·2594	4·2846	5·2218	6·2154
8	1·4083	2·3685	3·3641	4·5275	5·5994	6·5142
9	1·6770	2·5350	3·5912	4·6912	5·9705	6·9803
10	1·7090	2·6737	3·9078	4·8625	6·0880	7·2660

TABLE 7

Natural frequencies for single-layer 60° clamped and pinned piezoelectric shells ($h/a = 0{\cdot}01$)

Mode	N	1	2	3	4	5	6
P	edge						
1	Clamped	1·111	2·013	3·086	4·138	5·025	5·903
	Pinned	1·044	1·809	2·791	3·784	4·288	4·747
2	Clamped	1·318	2·270	2·464	4·579	5·357	6·101
	Pinned	1·281	2·215	3·413	4·133	5·152	6·071
3	Clamped	1·438	2·577	3·778	4·884	6·130	7·298
	Pinned	1·402	2·490	3·598	4·602	5·395	6·227
4	Clamped	1·704	2·884	4·133	5·405	6·792	7·731
	Pinned	1·644	2·838	3·843	4·885	6·168	7·433
5	Clamped	1·867	3·088	4·413	5·659	7·054	8·679
	Pinned	1·823	3·058	4·134	5·608	6·835	7·783

those of the 60° caps, and as much as 50% of those of the 45° shells, indicating that frequency is inversely proportional to the opening angle.

Natural frequencies for single-layer 60° clamped and pinned PZT-5 shells with a thickness-to-radius ratio 0·01 are calculated and shown in Table 7. In general, the frequencies of the pinned piezoelectric caps are around 8–12% less than the solutions of the clamped shells. As expected, the clamped piezoelectric shells are more rigid than the pinned caps, yet for many modes this influence is very small. This is especially true for the primary circumferential mode, for which the frequencies are very close. As the mode number increases, the differences also increase.

Free vibrations for single-layer 90° clamped piezoelectric shells with thickness-to-radius ratio 0·005, 0·01, 0·05 were also analyzed. The results are given in Table 8. The frequencies of the shells with thickness-to-radius ratio 0·005 are roughly 5–10% less than the ones of the caps with thickness-to-radius ratio 0·01, and the solutions of the caps with thickness-to-radius ratio 0·01 are about 5–10% less than the values of the shells with thickness-to-radius ratio 0·05. Hence, large increases in thickness do not yield commensurate increases in frequency.

Natural frequencies of two-layer clamped piezoelectric caps are computed for opening angle 45° to compare with the single-layer shells. The thickness-to-radius ratio (h/a) considered in this case is 0·005. The thicknesses of two layers are identical. The materials PZT-5 and (Pb) (CoW) TiO_3 are used for the two-layer piezoelectric shells. Their properties are listed in Table 4. The results can be seen from Table 9. Most values of the single-layer shells are about 10–12% larger than the two-layer caps.

Although most of our results focus on natural frequency, we also demonstrate the behavior of piezoelectric spherical shell mode shapes in free vibrations. The relative amplitude of 90° single-layer pinned caps are calculated from the eigenvectors and shown in Figure 5. The thickness-to-radius ratio (h/a) considered in the example is 0·005. The materials PZT-5 are used. These results are fairly typical, and show fairly regular behavior for v and w, but less uniform behavior for u.

Overall, the results of our study indicate that the first order shear deformation theory is more efficient than continuum theories and give good results for thin shells, because, in FSDT, it is assumed that the radius does not influence the results and can be ignored during integration. For example, the cases using FSDT have 110 degrees of freedom in our study, far less than the Ritz model in which 640 degrees of freedom are required. In general,

TABLE 8

Natural frequencies for single-layer 90° clamped piezoelectric shells with thickness-to-radius ratio

Mode N	1	2	3	4	5	6
P						
			(a) $h/a = 0{\cdot}005$			
1	0·6952	1·2751	1·8302	2·3153	2·8083	3·3785
2	0·9995	1·3985	2·1641	2·9058	3·5881	4·2992
3	1·0187	1·5883	2·3176	3·1858	3·8022	4·3844
4	1·0759	1·8071	2·5055	3·3240	4·4092	5·2794
5	1·1128	1·8569	2·6881	3·5190	4·5849	5·5003
6	1·2057	2·0286	2·9433	4·0137	4·8942	6·0745
7	1·2737	2·2512	3·2594	4·2846	5·2218	6·2154
8	1·4083	2·3685	3·3641	4·5275	5·5994	6·5142
9	1·6770	2·5350	3·5912	4·6912	5·9705	6·9803
10	1·7090	2·6737	3·9078	4·8625	6·0880	7·2660
			(b) $h/a = 0{\cdot}01$			
1	0·7068	1·4076	2·0211	2·5827	3·0978	3·6719
2	1·0453	1·5341	2·3039	3·1102	3·7970	4·3837
3	1·0840	1·6838	2·5727	3·2280	3·8666	4·5893
4	1·1901	1·8838	2·5950	3·5135	4·6308	5·4865
5	1·2638	2·0742	2·8017	3·6989	4·7270	5·5646
6	1·4040	2·2185	3·0803	4·1120	4·9491	6·2042
7	1·5080	2·3249	3·3645	4·4087	5·3781	6·3478
8	1·6971	2·5597	3·7319	4·7228	5·7002	6·6531
9	1·7547	2·8173	3·7511	4·8635	6·1643	7·0447
10	1·9269	3·0232	4·0334	5·1489	6·3699	7·5293
			(c) $h/a = 0{\cdot}05$			
1	0·7784	1·7886	2·5878	3·2185	3·8068	4·3855
2	1·3431	2·2532	3·1395	4·0926	4·8685	5·5097
3	1·5138	2·3565	3·4586	4·5412	5·4821	6·3561
4	1·7401	2·6138	3·6772	4·7151	5·8031	6·8435
5	1·9782	3·1303	4·0636	4·9858	6·0737	7·0293
6	2·1377	3·1873	4·3939	5·5158	6·3786	7·3391
7	2·4730	3·6051	4·5428	5·6795	6·7995	7·7861
8	2·8691	3·7868	5·0228	6·0001	6·9931	8·0517
9	3·0131	4·1958	5·3166	6·3180	7·4698	8·3932
10	3·4859	4·6369	5·5302	6·7593	7·7194	8·7871

piezoelectricity increases the frequency around 30% due to the increased stiffness. Because the shape of caps influences the vibration style, the frequencies are roughly inversely proportional to the opening angle of the shells. Also, the clamped piezoelectric shells are approximately 10% more rigid than the pinned caps caused by the change of boundary conditions.

4. CONCLUSIONS

We studied the dynamic behavior of homogeneous and layered elastic and piezoelectric caps in an attempt to develop both a general computational procedure of analysis and present, for what we believe is the first time, numerical results for layered piezoelectric spherical caps and indications of their behavior. Elastic shells were examined first to test the

TABLE 9

Comparison of natural frequencies between 45° single-layer and two-layer clamped piezoelectric shells ($h/a = 0{\cdot}005$)

Mode P	N	1	2	3	4	5	6
1	Single layer	1·264	2·251	3·520	4·764	5·818	6·943
	Two layer	1·270	2·158	3·327	4·551	5·550	6·560
2	Single layer	1·414	2·526	4·150	5·841	6·998	7·944
	Two layer	1·397	2·396	3·835	5·439	6·873	8·196
3	Single layer	1·605	2·971	4·766	6·055	7·410	8·868
	Two layer	1·565	2·771	4·527	6·263	7·869	9·778
4	Single layer	1·845	3·475	4·896	6·355	8·597	10·046
	Two layer	1·766	3·172	4·715	6·263	7·869	9·778
5	Single layer	1·845	3·848	5·194	7·037	8·838	10·836
	Two layer	1·957	3·664	5·139	6·513	8·146	10·169

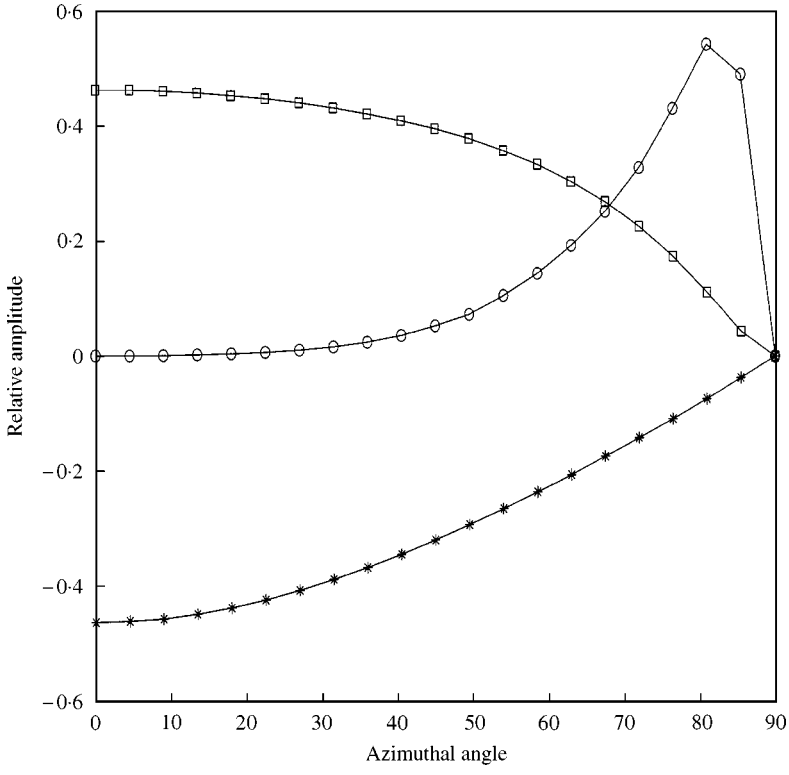

Figure 5. Relative amplitude for 90° single-layer pinned piezoelectric caps: $h/a = 0{\cdot}005$, Mode = 1. ○, U; □, V; *, W.

accuracy of the formulation. In the elastic cases, frequencies of various angles of caps were calculated with first order deformation theory and were in close agreement with results from other studies. The solutions for piezoelectric shells, which have not been studied previously, will provide a means of comparison for other techniques and methods. The numerical model developed in this study can be used in a wide variety of applications including

deformation calculation of smart membranes and active shells, frequency analysis of laminated transducers and sensors, and the design of artificial heart pumps and robotic surgery instruments.

REFERENCES

1. P. M. NAGHDI 1957 *Quarterly of Applied Mathematics* **15**, 41–52. The effect of transverse shear deformation on the bending of elastic shells of revolution.
2. P. M. NAGHDI 1957 *Quarterly of Applied Mathematics* **14**, 369–380. On the theory of thin elastic shells.
3. W. M. JOHNSON and E. REISSNER 1958 *Quarterly of Applied Mathematics* **15**, 367–380. On transverse vibrations of shallow spherical shells.
4. W. H. HOPPMANN 1961 *Journal of Applied Mechanics* 305–307. Frequencies of vibration of shallow spherical shells.
5. P. M. NAGHDI and A. KALNINS 1962 *Journal of Applied Mechanics* 65–72. On vibrations of elastic spherical shells.
6. J. J. MUKHER 1968 *American Institute of Aeronautics and Astronautics Journal* **6**, 1563–1565. Stresses due to vibration of spherical shells of aeolotropic materials.
7. C. PRASAD 1964 *The Journal of the Acoustical Society of America* **36**, 489–494. On vibrations of spherical shells.
8. A. KALNINS 1964 *The Journal of the Acoustical Society of America* **36**, 74–81. Effect of bending on vibrations of spherical shells.
9. M. S. ZARGHAMEE and A. R. ROBINSON 1967 *American Institute of Aeronautics and Astronautics Journal* **5**, 1256–1261. A numerical method for analysis of free vibration of spherical shells.
10. B. K. RATH and Y. C. DAS 1973 *Journal of Sound and Vibration* **28**, 737–757. Vibration of layered shells.
11. B. K. RATH and Y. C. DAS 1973 *Journal of Sound and Vibration* **37**, 123–136. Axisymmetric vibration of closed layered spherical shells.
12. J. VENKATARAMANA and R. G. VENKATESWARA 1975 *Nuclear Engineering and Design* **33**, 398–402. Finite element analysis of moderately thick shells.
13. V. C. M. DE SOUZA and J. G. A. CROLL 1980 *Journal of Sound and Vibration* **73**, 379–404. An energy analysis of the free vibrations of isotropic spherical shells.
14. H. KUNIEDA 1984 *Journal of Sound and Vibration* **92**, 1–10. Flexural axisymmetric free vibrations of a spherical dome: exact results and approximate solutions.
15. A. V. SINGH and S. MIRZA 1985 *Journal of Pressure Vessel Technology* **107**, 77–82. Asymmetric modes and associated eigenvalues for spherical shells.
16. A. TESSLER and L. SPIRIDIGLIOZZI 1988 *International Journal for Numerical Methods in Engineering* **26**, 1071–1086. Resolving memberane and shear locking phenomena in curved shear-deformable axisymmetric shell elements.
17. C. C. CHAO, T. P. TUNG and Y. C. CHERN 1991 *Journal of Vibration and Acoustics* **113**, 152–159. Axisymmetric free vibration of thick orthotropic hemispherical shells under various edge conditions.
18. B. P. GAUTHAM and N. GANESAN 1997 *Journal of Sound and Vibration* **204**, 17–40. Free vibration characteristics of isotropic and laminated orthotropic spherical caps.
19. P. HEYLIGER and Y. C. WU 1999 *International Journal of Engineering Science* **32**, 143–161. Electroelastic fields in layered piezoelectric spheres.
20. H. F. TIERSTEN 1969 *Linear Piezoelectric Plate Vibrations*. New York: Plenum.
21. Y. C. FUNG 1965 *Foundations of Solid Mechanics*. NJ: Englewood Cliffs.
22. P. HEYLIGER 2000 *Journal of Acoustic Society* **107**, 1–10. Traction-free vibration of layered elastic and piezoelectric rectangular parallelepipeds.

APPENDIX A: ELEMENTS OF THE COEFFICIENT MATRICES

The elements of the coefficient matrices for the first order shear deformation method are expressed as

$$M_{ij}^{11} = \int_{\zeta}\int_{\theta} [A_{11}\psi_j^{\hat{u}}\psi_i^{\hat{u}}]\, r^2 \sin\zeta \,\mathrm{d}\theta\,\mathrm{d}\zeta, \qquad M_{ij}^{22} = \int_{\zeta}\int_{\theta} [A_{22}\psi_j^{\hat{v}}\psi_i^{\hat{v}}]\, r^2 \sin\zeta \,\mathrm{d}\theta\,\mathrm{d}\zeta,$$

$$M_{ij}^{33} = \int_\zeta \int_\theta [A_{33}\psi_j^{\hat{w}}\psi_i^{\hat{w}}] \sin\zeta \, \mathrm{d}\theta \, \mathrm{d}\zeta, \qquad M_{ij}^{44} = \int_\zeta \int_\theta [A_{44}\psi_j^{\hat{\alpha}}\psi_i^{\hat{\alpha}}] \, r^2 \sin\zeta \, \mathrm{d}\theta \, \mathrm{d}\zeta,$$

$$M_{ij}^{55} = \int_\zeta \int_\theta [A_{55}\psi_j^{\hat{\beta}}\psi_i^{\hat{\beta}}] \, r^2 \sin\zeta \, \mathrm{d}\theta \, \mathrm{d}\zeta, \qquad M_{ij}^{24} = \int_\zeta \int_\theta [A_{24}\psi_j^{\hat{\alpha}}\psi_i^{\hat{v}}] \, r^2 \sin\zeta \, \mathrm{d}\theta \, \mathrm{d}\zeta,$$

$$M_{ij}^{35} = \int_\zeta \int_\theta [A_{35}\psi_i^{\hat{w}}\psi_j^{\hat{\beta}}] \, r^2 \sin\zeta \, \mathrm{d}\theta \, \mathrm{d}\zeta,$$

$$K_{ij}^{11} = \int_\zeta \int_\theta \Bigg[E_{11} \frac{\psi_j^{\hat{u}}}{r} \frac{\psi_i^{\hat{u}}}{r} + E_{12} \frac{\psi_j^{\hat{u}}}{r} \frac{\psi_i^{\hat{u}}}{r} + E_{21} \frac{\psi_j^{\hat{u}}}{r} \frac{\psi_i^{\hat{u}}}{r} + E_{22} \frac{\psi_j^{\hat{u}}}{r} \frac{\psi_i^{\hat{u}}}{r} + E_{44} \frac{\partial\psi_j^{\hat{u}}}{r\partial\zeta} \frac{\partial\psi_i^{\hat{u}}}{r\partial\zeta}$$
$$+ E_{55} \frac{1}{r^2 \sin^2\zeta} \frac{\partial\psi_j^{\hat{u}}}{\partial\theta} \frac{\partial\psi_i^{\hat{u}}}{\partial\theta} \Bigg] r^2 \sin\zeta \, \mathrm{d}\theta \, \mathrm{d}\zeta,$$

$$K_{ij}^{12} = \int_\zeta \int_\theta \Bigg[E_{11} \frac{\partial\psi_j^{\hat{v}}}{r\partial\zeta} \frac{\psi_i^{\hat{u}}}{r} + E_{12} \frac{\cos\zeta}{r\sin\zeta} \psi_j^{\hat{v}} \frac{\psi_i^{\hat{u}}}{r} + E_{21} \frac{\partial\psi_j^{\hat{v}}}{r\partial\zeta} \frac{\psi_i^{\hat{u}}}{r} + E_{22} \frac{\cos\zeta}{r\sin\zeta} \psi_j^{\hat{v}} \frac{\psi_i^{\hat{u}}}{r}$$
$$- E_{44} \frac{\psi_j^{\hat{v}}}{r} \frac{\partial\psi_i^{\hat{u}}}{r\partial\zeta} \Bigg] r^2 \sin\zeta \, \mathrm{d}\theta \, \mathrm{d}\zeta,$$

$$K_{ij}^{13} = \int_\zeta \int_\theta \Bigg[E_{12} \frac{1}{r\sin\zeta} \frac{\partial\psi_j^{\hat{w}}}{\partial\theta} \frac{\psi_i^{\hat{u}}}{r} + E_{22} \frac{1}{r\sin\zeta} \frac{\partial\psi_j^{\hat{w}}}{\partial\theta} \frac{\psi_i^{\hat{u}}}{r} - E_{55} \frac{\psi_j^{\hat{w}}}{r} \frac{1}{r\sin\zeta} \frac{\partial\psi_i^{\hat{u}}}{\partial\theta} \Bigg] r^2 \sin\zeta \, \mathrm{d}\theta \, \mathrm{d}\zeta,$$

$$K_{ij}^{14} = \int_\zeta \int_\theta \Bigg[E_{61} \frac{\partial\psi_j^{\hat{\alpha}}}{r\partial\zeta} \frac{\psi_i^{\hat{u}}}{r} + E_{62} \frac{\partial\psi_j^{\hat{\alpha}}}{r\partial\zeta} \frac{\psi_i^{\hat{u}}}{r} + E_{71} \frac{\cos\zeta}{r\sin\zeta} \psi_j^{\hat{\alpha}} \frac{\psi_i^{\hat{u}}}{r} + E_{72} \frac{\cos\zeta}{r\sin\zeta} \psi_j^{\hat{\alpha}} \frac{\psi_i^{\hat{u}}}{r}$$
$$+ E_{44} \psi_j^{\hat{\alpha}} \frac{\partial\psi_i^{\hat{u}}}{r\partial\zeta} \Bigg] r^2 \sin\zeta \, \mathrm{d}\theta \, \mathrm{d}\zeta,$$

$$K_{ij}^{15} = \int_\zeta \int_\theta \Bigg[E_{71} \frac{1}{r\sin\zeta} \frac{\partial\psi_j^{\hat{\beta}}}{\partial\theta} \frac{\psi_i^{\hat{u}}}{r} + E_{72} \frac{1}{r\sin\zeta} \frac{\partial\psi_j^{\hat{\beta}}}{\partial\theta} \frac{\psi_i^{\hat{u}}}{r} + E_{55} \frac{1}{r\sin\zeta} \frac{\partial\psi_i^{\hat{u}}}{\partial\theta} \psi_j^{\hat{\beta}} \Bigg] r^2 \sin\zeta \, \mathrm{d}\theta \, \mathrm{d}\zeta,$$

$$K_{ij}^{16} = \int_\zeta \int_\theta \Bigg[E_{59} \frac{1}{r^2} \frac{\partial\psi_i^{\hat{u}}}{\partial\zeta} \frac{\partial\psi_j^{\hat{\phi}}}{\partial\zeta} + E_{30} \frac{1}{r^2 \sin^2\zeta} \frac{\partial\psi_i^{\hat{u}}}{\partial\theta} \frac{\partial\psi_j^{\hat{\phi}}}{\partial\theta} \Bigg] r^2 \sin\zeta \, \mathrm{d}\theta \, \mathrm{d}\zeta,$$

$$K_{ij}^{22} = \int_\zeta \int_\theta \Bigg[E_{11} \frac{\partial\psi_j^{\hat{v}}}{r\partial\zeta} \frac{\partial\psi_i^{\hat{v}}}{\partial\zeta} + E_{12} \frac{\cos\zeta}{r\sin\zeta} \psi_j^{\hat{v}} \frac{\partial\psi_i^{\hat{v}}}{r\partial\zeta} + E_{21} \frac{\partial\psi_j^{\hat{v}}}{r\partial\zeta} \frac{\cos\zeta}{r\sin\zeta} \psi_i^{\hat{v}} + E_{22} \frac{\cos^2\zeta}{r^2\sin^2\zeta} \psi_j^{\hat{v}} \psi_i^{\hat{v}}$$
$$+ E_{44} \frac{\psi_j^{\hat{v}}\psi_i^{\hat{v}}}{r^2} + E_{33} \frac{1}{r^2\sin^2\zeta} \frac{\partial\psi_j^{\hat{v}}}{\partial\theta} \frac{\partial\psi_i^{\hat{v}}}{\partial\theta} \Bigg] r^2 \sin\zeta \, \mathrm{d}\theta \, \mathrm{d}\zeta,$$

$$K_{ij}^{23} = \int_\zeta \int_\theta \Bigg[E_{12} \frac{1}{r\sin\zeta} \frac{\partial\psi_j^{\hat{w}}}{\partial\theta} \frac{\partial\psi_i^{\hat{v}}}{r\partial\zeta} + E_{22} \frac{\cos\zeta}{r^2\sin^2\zeta} \frac{\partial\psi_j^{\hat{w}}}{\partial\theta} \psi_i^{\hat{v}}$$
$$+ E_{33} \left(\frac{\partial\psi_j^{\hat{w}}}{r\partial\zeta} \frac{1}{r\sin\zeta} \frac{\partial\psi_i^{\hat{v}}}{\partial\theta} - \frac{\cos\zeta}{r\sin\zeta} \psi_j^{\hat{w}} \frac{1}{r\sin\zeta} \frac{\partial\psi_i^{\hat{v}}}{\partial\theta} \right) \Bigg] r^2 \sin\zeta \, \mathrm{d}\theta \, \mathrm{d}\zeta,$$

$$K_{ij}^{24} = \int_\zeta \int_\theta \Bigg[E_{61} \frac{\partial \psi_j^{\hat{z}}}{r\partial\zeta} \frac{\partial \psi_i^{\hat{v}}}{r\partial\zeta} + E_{62} \frac{\partial \psi_j^{\hat{z}}}{r\partial\zeta} \frac{\cos\zeta}{r\sin\zeta} \psi_i^{\hat{v}} + E_{72} \frac{\cos\zeta}{r\sin\zeta} \psi_j^{\hat{z}} \frac{\cos\zeta}{r\sin\zeta} \psi_i^{\hat{v}} - E_{44} \frac{\psi_j^{\hat{v}}}{r} \psi_i^{\hat{z}}$$

$$+ E_{38} \frac{1}{r^2 \sin^2\zeta} \frac{\partial \psi_j^{\hat{z}}}{\partial\theta} \frac{\partial \psi_i^{\hat{v}}}{\partial\theta} \Bigg] r^2 \sin\zeta \, \mathrm{d}\theta \, \mathrm{d}\zeta,$$

$$K_{ij}^{25} = \int_\zeta \int_\theta \Bigg[E_{71} \frac{1}{r\sin\zeta} \frac{\partial \psi_j^{\hat{\beta}}}{\partial\theta} \frac{\partial \psi_i^{\hat{v}}}{r\partial\zeta} + E_{72} \frac{1}{r\sin\zeta} \frac{\partial \psi_j^{\hat{\beta}}}{\partial\theta} \frac{\cos\zeta}{r\sin\zeta} \psi_i^{\hat{v}}$$

$$+ E_{83} \left(\frac{1}{r^2\sin\zeta} \frac{\partial \psi_i^{\hat{v}}}{\partial\theta} \frac{\partial \psi_j^{\hat{\beta}}}{\partial\zeta} - \frac{\cos\zeta}{r^2\sin^2\zeta} \frac{\partial \psi_i^{\hat{v}}}{\partial\theta} \psi_j^{\hat{\beta}} \right) \Bigg] r^2 \sin\zeta \, \mathrm{d}\theta \, \mathrm{d}\zeta,$$

$$K_{ij}^{26} = \int_\zeta \int_\theta \Bigg[- E_{59} \frac{1}{r^2} \psi_i^{\hat{v}} \frac{\partial \psi_j^{\hat{\phi}}}{\partial\zeta} \Bigg] r^2 \sin\zeta \, \mathrm{d}\zeta \, \mathrm{d}\theta,$$

$$K_{ij}^{33} = \int_\zeta \int_\theta \Bigg[E_{22} \frac{1}{r^2\sin^2\zeta} \frac{\partial \psi_j^{\hat{w}}}{\partial\theta} \frac{\partial \psi_i^{\hat{w}}}{\partial\theta}$$

$$+ E_{33} \left(\frac{\partial \psi_j^{\hat{w}}}{r\partial\zeta} \frac{\partial \psi_i^{\hat{w}}}{r\partial\zeta} - \frac{\partial \psi_j^{\hat{w}}}{r\partial\zeta} \frac{\cos\zeta}{r\sin\zeta} \psi_i^{\hat{w}} - \frac{\cos\zeta}{r\sin\zeta} \psi_j^{\hat{w}} \frac{\partial \psi_i^{\hat{w}}}{r\partial\zeta} \right.$$

$$\left. + \frac{\cos\zeta}{r\sin\zeta} \psi_j^{\hat{w}} \frac{\cos\zeta}{r\sin\zeta} \psi_i^{\hat{w}} \right) + E_{55} \frac{\psi_j^{\hat{w}}}{r} \frac{\psi_i^{\hat{w}}}{r} \Bigg] r^2 \sin\zeta \, \mathrm{d}\theta \, \mathrm{d}\zeta,$$

$$K_{ij}^{34} = \int_\zeta \int_\theta \Bigg[E_{62} \frac{\partial \psi_j^{\hat{z}}}{r\partial\zeta} \frac{1}{r\sin\zeta} \frac{\partial \psi_i^{\hat{w}}}{\partial\theta} + E_{72} \frac{\cos\zeta}{r\sin\zeta} \psi_j^{\hat{z}} \frac{1}{r\sin\zeta} \frac{\partial \psi_i^{\hat{w}}}{\partial\theta}$$

$$+ E_{38} \left(\frac{1}{r\sin\zeta} \frac{\partial \psi_j^{\hat{z}}}{\partial\theta} \frac{\partial \psi_i^{\hat{w}}}{r\partial\zeta} - \frac{1}{r\sin\zeta} \frac{\partial \psi_j^{\hat{z}}}{\partial\theta} \frac{\cos\zeta}{r\sin\zeta} \psi_i^{\hat{w}} \right) \Bigg] r^2 \sin\zeta \, \mathrm{d}\theta \, \mathrm{d}\zeta,$$

$$K_{ij}^{35} = \int_\zeta \int_\theta \Bigg[E_{27} \frac{1}{r^2\sin^2\zeta} \frac{\partial \psi_j^{\hat{\beta}}}{\partial\theta} \frac{\partial \psi_i^{\hat{w}}}{\partial\theta}$$

$$+ E_{38} \left(\frac{\partial \psi_j^{\hat{\beta}}}{r\partial\zeta} \frac{\partial \psi_i^{\hat{w}}}{r\partial\zeta} - \frac{\partial \psi_j^{\hat{\beta}}}{r\partial\zeta} \frac{\cos\zeta}{r\sin\zeta} \psi_i^{\hat{w}} - \frac{\cos\zeta}{r\sin\zeta} \psi_j^{\hat{\beta}} \frac{\partial \psi_i^{\hat{w}}}{r\partial\zeta} \right.$$

$$\left. + \frac{\cos\zeta}{r\sin\zeta} \psi_j^{\hat{\beta}} \frac{\cos\zeta}{r\sin\zeta} \psi_i^{\hat{w}} \right) - E_{55} \psi_j^{\hat{\beta}} \frac{\psi_i^{\hat{w}}}{r} \Bigg] r^2 \sin\zeta \, \mathrm{d}\theta \, \mathrm{d}\zeta,$$

$$K_{ij}^{36} = \int_\zeta \int_\theta \Bigg[- E_{30} \frac{1}{r^2\sin\zeta} \psi_i^{\hat{w}} \frac{\partial \psi_j^{\hat{\phi}}}{\partial\theta} \Bigg] r^2 \sin\zeta \, \mathrm{d}\theta \, \mathrm{d}\zeta,$$

$$K_{ij}^{44} = \int_\zeta \int_\theta \Bigg[E_{67} \frac{\cos\zeta}{r\sin\zeta} \psi_j^{\hat{z}} \frac{\partial \psi_i^{\hat{z}}}{r\partial\zeta} + E_{76} \frac{\partial \psi_j^{\hat{z}}}{r\partial\zeta} \frac{\cos\zeta}{r\sin\zeta} \psi_i^{\hat{z}} + E_{77} \frac{\cos^2\zeta}{r^2\sin^2\zeta} \psi_j^{\hat{z}} \psi_i^{\hat{z}} + E_{44} \psi_j^{\hat{z}} \psi_i^{\hat{z}}$$

$$+ E_{88} \frac{1}{r^2\sin^2\zeta} \frac{\partial \psi_j^{\hat{z}}}{\partial\theta} \frac{\partial \psi_i^{\hat{z}}}{\partial\theta} + E_{66} \frac{\partial \psi_j^{\hat{z}}}{r\partial\zeta} \frac{\partial \psi_i^{\hat{z}}}{r\partial\zeta} \Bigg] r^2 \sin\zeta \, \mathrm{d}\theta \, \mathrm{d}\zeta,$$

$$K_{ij}^{45} = \int_{\zeta}\int_{\theta}\left[E_{76}\frac{\partial\psi_j^{\hat{\alpha}}}{r\partial\zeta}\frac{1}{r\sin\zeta}\frac{\partial\psi_i^{\hat{\beta}}}{\partial\theta} + E_{77}\frac{\cos\zeta}{r\sin\zeta}\psi_j^{\hat{\alpha}}\frac{1}{r\sin\zeta}\frac{\partial\psi_i^{\hat{\beta}}}{\partial\theta}\right.$$
$$\left. + E_{88}\left(\frac{1}{r\sin\zeta}\frac{\partial\psi_j^{\hat{\alpha}}}{\partial\theta}\frac{\partial\psi_i^{\hat{\beta}}}{r\partial\zeta} - \frac{1}{r\sin\zeta}\frac{\partial\psi_j^{\hat{\alpha}}}{\partial\theta}\frac{\cos\zeta}{r\sin\zeta}\psi_i^{\hat{\beta}}\right)\right] r^2\sin\zeta\,\mathrm{d}\theta\,\mathrm{d}\zeta,$$

$$K_{ij}^{46} = \int_{\zeta}\int_{\theta}\left[E_{59}\frac{1}{r}\psi_i^{\hat{\alpha}}\frac{\partial\psi_j^{\hat{\phi}}}{\partial\zeta}\right] r^2\sin\zeta\,\mathrm{d}\theta\,\mathrm{d}\zeta,$$

$$K_{ij}^{55} = \int_{\zeta}\int_{\theta}\left[E_{77}\frac{1}{r\sin\zeta}\frac{\partial\psi_j^{\hat{\beta}}}{\partial\theta}\frac{1}{r\sin\zeta}\frac{\partial\psi_i^{\hat{\beta}}}{\partial\theta}\right.$$
$$+ E_{88}\left(\frac{\partial\psi_j^{\hat{\beta}}}{r\partial\zeta}\frac{\partial\psi_i^{\hat{\beta}}}{r\partial\zeta} - \frac{\partial\psi_j^{\hat{\beta}}}{r\partial\zeta}\frac{\cos\zeta}{r\sin\zeta}\psi_i^{\hat{\beta}} - \frac{\cos\zeta}{r\sin\zeta}\psi_j^{\hat{\beta}}\frac{\partial\psi_i^{\hat{\beta}}}{r\partial\zeta}\right.$$
$$\left.\left. + \frac{\cos^2\zeta}{r^2\sin^2\zeta}\psi_j^{\hat{\beta}}\psi_i^{\hat{\beta}}\right)\right] r^2\sin\zeta\,\mathrm{d}\theta\,\mathrm{d}\zeta,$$

$$K_{ij}^{56} = \int_{\zeta}\int_{\theta}\left[E_{30}\frac{1}{r\sin\zeta}\psi_i^{\hat{\beta}}\frac{\partial\psi_j^{\hat{\phi}}}{\partial\theta}\right] r^2\sin\zeta\,\mathrm{d}\theta\,\mathrm{d}\zeta,$$

$$K_{ij}^{66} = \int_{\zeta}\int_{\theta}\left[-E_{99}\frac{1}{r^2}\frac{\partial\psi_i^{\hat{\phi}}}{\partial\zeta}\frac{\partial\psi_j^{\hat{\phi}}}{\partial\zeta} - E_{00}\frac{1}{r^2\sin^2\zeta}\frac{\partial\psi_i^{\hat{\phi}}}{\partial\theta}\frac{\partial\psi_j^{\hat{\phi}}}{\partial\theta}\right] r^2\sin\zeta\,\mathrm{d}\theta\,\mathrm{d}\zeta.$$

A specific problem for the use of spherical co-ordinate relates to the value of $1/\sin\xi$, which goes to infinity when ζ is zero. In the past study [15], a small circular hole was introduced to alleviate this problem, with the integration taken up to this point in the area integral. In the present study, we used Gaussian integration. Because Gaussian quadrature points avoid the apex, the difficulty of the singularity was avoided.